Oncogene (2019) 38:4915–4931
https://doi.org/10.1038/s41388-019-0764-z

ARTICLE

Sirtuin-mediated deacetylation of hnRNP A1 suppresses glycolysis and growth in hepatocellular carcinoma

Hao Yang[1,2] · Rongxuan Zhu[3] · Xiaoping Zhao[2] · Liu Liu[4] · Zhaoli Zhou[1] · Li Zhao[2] · Beibei Liang[1] · Wenjing Ma[1] · Jian Zhao[5] · Jianjun Liu[2] · Gang Huang[1,2]

Received: 14 August 2018 / Revised: 25 January 2019 / Accepted: 16 February 2019 / Published online: 11 March 2019

Abstract

Tumor cells undergo a metabolic shift in order to adapt to the altered microenvironment, although the underlying mechanisms have not been fully explored. HnRNP A1 is involved in the alternative splicing of the pyruvate kinase (*PK*) mRNA, allowing tumor cells to specifically produce the PKM2 isoform. We found that the acetylation status of hnRNP A1 in hepatocellular carcinoma (HCC) cells was dependent on glucose availability, which affected the PKM2-dependent glycolytic pathway. In the glucose-starved HCC cells, SIRT1 and SIRT6, members of deacetylase sirtuin family, were highly expressed and deacetylated hnRNP A1 after direct binding. We identified four lysine residues in hnRNP A1 that were deacetylated by SIRT1 and SIRT6, resulting in significant inhibition of glycolysis in HCC cells. Deacetylated hnRNP A1 reduced PKM2 and increased PKM1 alternative splicing in HCC cells under normal glucose conditions, thereby reducing the metabolic activity of PK and the non-metabolic PKM2–β-catenin signaling pathway. However, under glucose starvation, the low levels of acetylated hnRNP A1 reduced HCC cell metabolism to adapt to the nutrient deficiency. Taken together, sirtuin-mediated hnRNP A1 deacetylation inhibits HCC cell proliferation and tumorigenesis in a PKM2-dependent manner. These findings point to the metabolic reprogramming induced by hnRNP A1 acetylation in order to adapt to the nutritional status of the tumor microenvironment.

Introduction

Tumor cells are characterized by a high glucose uptake and glycolysis under aerobic and hypoxic conditions, a phenomenon known as the Warburg effect [1]. This aberrant glucose metabolism in tumor cells is largely attributed to the abnormal activity and function of glycolytic enzymes, including hexokinase 2 (HK2), phosphofructokinase (PFK), pyruvate kinase (PK), and lactate dehydrogenase (LDH) [2]. PK plays an important role in tumor metabolism, and PKM1 and PKM2 are its two isozymes that respectively promote oxidative phosphorylation and aerobic glycolysis. The heterogeneous nuclear ribonucleoprotein (hnRNP) A1, hnRNP A2/B1, and PTB are known to regulate the expression of PKM2, but not PKM1, in tumor cells [3, 4]. HnRNP A1 mediates DNA repair, RNA splicing, telomere elongation, and cell signal transduction in tumorigenesis [5, 6], and is expressed at high levels in different tumor cells [7–9]. HnRNP A1 binds to the 5' splice site (EI9) of *PKM* pre-mRNA exon 9, which leads to the excision of exon 9 and formation of *PKM2* mRNA, which is expressed at high levels in tumor cells. *PKM1* is the main PK isoform in

These authors contributed equally: Hao Yang, Rongxuan Zhu

Supplementary information The online version of this article (https://doi.org/10.1038/s41388-019-0764-z) contains supplementary material, which is available to authorized users.

✉ Jianjun Liu
nuclearj@163.com

✉ Gang Huang
huanggang@sumhs.edu.cn

[1] Shanghai Key Laboratory of Molecular Imaging, Shanghai University of Medicine and Health Sciences, Shanghai 201318, China

[2] Department of Nuclear Medicine, Ren Ji Hospital, Shanghai Jiao Tong University School of Medicine, Shanghai 200127, China

[3] Department of Oncology, Shanghai General Hospital, Shanghai Jiao Tong University School of Medicine, Shanghai 200080, China

[4] Department of Nuclear Medicine, Shanghai Chest Hospital, Shanghai Jiao Tong University, Shanghai 200030, China

[5] International Joint Cancer Institute, The Second Military Medical University, Shanghai 200433, China

normal differentiated cells, which is the result of alternative splicing by hnRNP A1 that excludes exon 10 [10, 11]. PKM2 not only enhances the accumulation of glycolysis-related metabolites in the tumor cells, but also acts as a coactivator of transcription factors such as HIF-1α and β-catenin to promote signal transduction and tumorigenesis [12–15].

Sirtuins belong to a family of protein deacetylases that includes seven homologs in mammals (SIRT1 to SIRT7). Studies show that sirtuins regulate mitochondrial biosynthesis, fatty acid oxidation, and gene transcription in hepatocellular carcinoma (HCC) and other cancers [16, 17]. For example, SIRT1 deacetylated p53 and decreased glucose uptake in cancer cells, resulting in increased mitochondrial respiration [18]. SIRT6-mediated deacetylation of H3K9 regulated the expression of various glycolytic genes and suppressed HIF-1α transcriptional activity [19]. Furthermore, SIRT2 and SIRT6 deacetylated PKM2 at the K305 and K433 residues, and reduced PKM2-mediated tumor metabolism in tumor cells [20, 21]. However, the exact role of sirtuin-dependent deacetylation of hnRNP A1, hnRNP A2/B1, or PTB in tumor metabolism is largely unknown. We hypothesized that the highly expressed hnRNP A1 in HCC cells was deacetylated by sirtuins, which inhibited the alternative splicing of PKM2, and therefore altered the cellular metabolism. Our results show that increased sirtuin expression under stress conditions such as glucose starvation promoted the deacetylation of hnRNP A1 and reduced glycolysis and proliferation of HCC cells to help them adapt to the nutrient deficiency.

Results

High expression of hnRNP A1 is predictive of HCC progression and poor prognosis

The in situ expression of hnRNP A1 in HCC and adjacent non-cancerous tissues was analyzed in 78 HCC patients and was found to be significantly higher in the tumor tissues (Fig. 1a, b). Based on the expression levels of hnRNP A1, the patients were classified into the high ($n = 52$)- and low ($n = 26$)-expressing groups, and high levels of hnRNP A1 were associated with higher tumor stages ($p = 0.021$) and larger tumors ($p = 0.037$; Table 1), as well as poor prognosis ($p = 0.0057$; Fig. 1c). In addition, we also found a positive correlation between high hnRNP A1 expression and the expression of β-catenin ($p = 0.025$) and glypican-3 ($p = 0.038$), the main biopsy markers in HCC (Table 2). Analyses of the expression levels in randomly selected tissues revealed significantly higher expression of both hnRNP A1 and its effector PKM2 in HCC than in normal tissues (Supplementary Fig. 1a). Meanwhile, the gene-expression level in several tumor types was detected by GEPIA network tool. The results showed that the mRNA expression of *hnRNP A1* and *PKM* in liver hepatocellular cancer was higher than that in normal tissues (Fig. 1d, Supplementary Fig. 1b). Taken together, high hnRNP A1 expression in HCC is likely correlated to more aggressive tumor characteristics.

Sirtuins deacetylate and interact with hnRNP A1

In addition to its own expression level, we also found that the expression of acetylated hnRNP A1 in human HCC tissues was higher than that in adjacent tissues (Supplementary Fig. 1a). HepG2 cells overexpressing FLAG-tagged hnRNP A1 were treated with either the HDAC inhibitor trichostatin A (TSA, 5 μM) or the sirtuin inhibitor nicotinamide (NAM, 10 nM). Treatment with NAM significantly increased the acetylation of hnRNP A1 (Fig. 2a), thus confirming that the latter was deacetylated by sirtuins. To determine which sirtuins deacetylated hnRNP A1, we co-transfected HepG2, 293T, HCT116, and A549 cells with FLAG-hnRNP A1 and different HA-tagged sirtuins (except SIRT3 and SIRT4 since they are only expressed in the mitochondria [22]). Both HA-SIRT1 and HA-SIRT6 significantly deacetylated FLAG-hnRNP A1, as reflected in the decreased levels of lysine-acetylated hnRNP A1 (Fig. 2b, Supplementary Fig. 2a). The expression of SIRT1 and SIRT6 in tumor and normal tissues differed little in the GEPIA database (Supplementary Fig. 2b and 2c); so, we hypothesized that sirtuins regulate the deacetylation of hnRNP A1 conditionally.

Since previous studies have shown that glucose starvation leads to the activation and increased expression of SIRT1 and SIRT6 [21, 23], we examined the acetylation level of hnRNP A1 under glucose starvation. HepG2, 293T, HCT116, and A549 cells were cultured in 5 mM glucose for 0, 12, and 24 h, which significantly increased SIRT1 and SIRT6 protein levels, and subsequently led to a decrease in hnRNP A1 acetylation (Fig. 2c, Supplementary Fig. 2d). HepG2 cells were treated with selective inhibitors of SIRT1 (EX527) or SIRT6 (Compound 9 [24]), and each resulted in increased hnRNP A1 acetylation (Fig. 2d). The co-immunoprecipitation (co-IP) of the endogenous hnRNP A1 protein and SIRT1 or SIRT6 in the HCC cells indicated their direct physical interaction (Fig. 2e) and was further validated by silver-staining assay and mass spectrometry (Fig. 2f, Supplementary Table 1), which showed FLAG-hnRNP A1 binding to SIRT1 (located at 82 kD) and SIRT6 (located at 39 kD). Moreover, glucose starvation further amplified the interaction between hnRNP A1 and SIRT1 or SIRT6 (Fig. 2g), implying that glucose starvation inhibited hnRNP A1 acetylation. Immunofluorescence assay showed

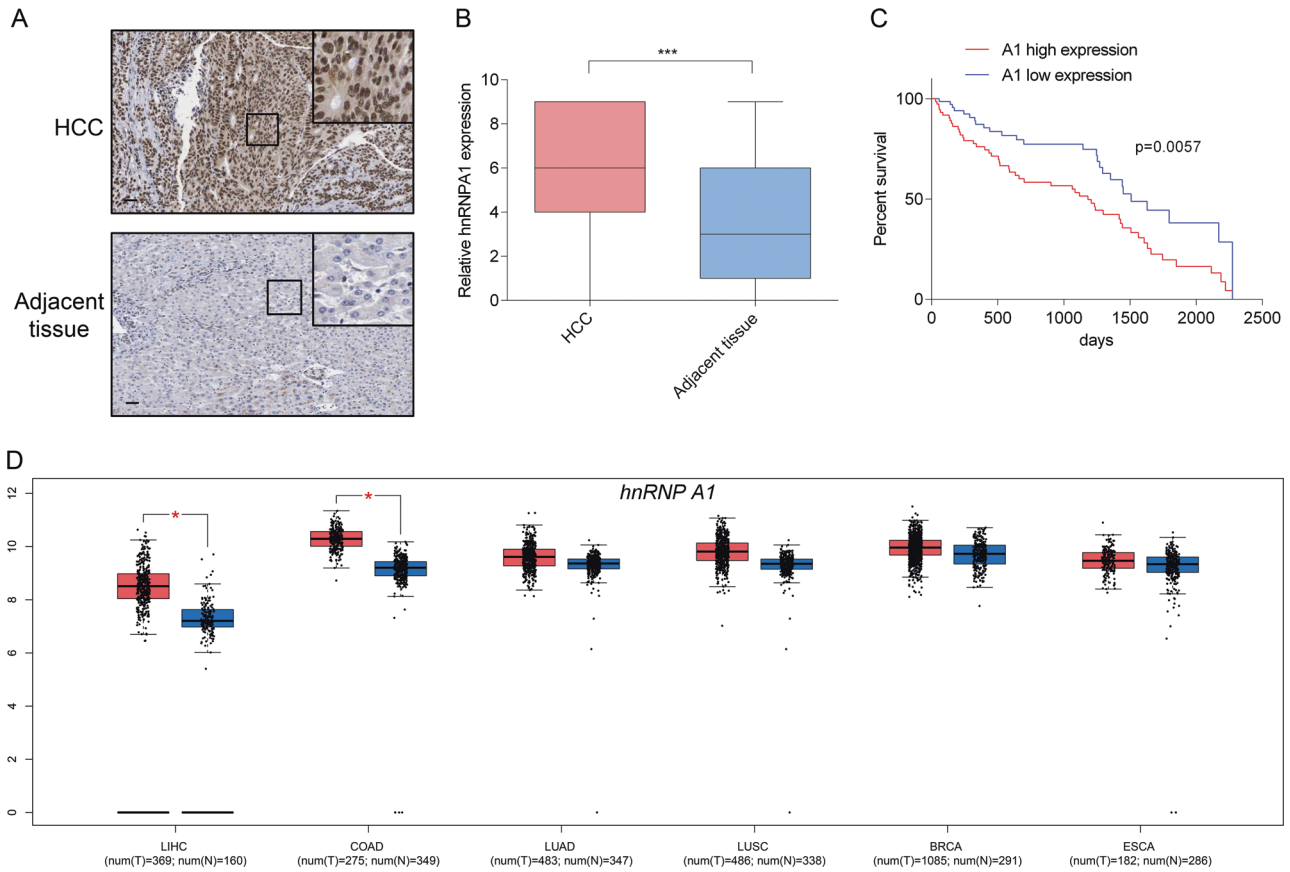

Fig. 1 HnRNP A1 was highly expressed in HCC and predicted poor prognosis. **a** Representative IHC images of tumors (upper) and adjacent normal tissues (lower) showing hnRNP A1 expression (scale bar, 50 μm). **b** Statistical analysis of IHC scores for 78 HCC tumors and adjacent normal tissues. ***p <0.001. **c** Survival curves of 52 hnRNP A1 high-expressing (red) and 26 low-expressing (blue) patients. **d** The expression of *hnRNP A1* mRNA in different types of cancer was analyzed by the GEPIA network tool. T: tumor (red); N: normal tissue (blue). LIHC, liver hepatocellular carcinoma; COAD, colon adenocarcinoma; LUAD, lung adenocarcinoma; LUSC, lung squamous cell carcinoma; BRCA, breast invasive carcinoma; ESCA, esophageal carcinoma; HCC, hepatocellular carcinoma; IHC, immunohistochemistry

significantly increased co-localization of hnRNP A1 and SIRT1 or SIRT6 under glucose starvation compared to normal culture conditions (25 mM glucose) in HepG2 cells (Fig. 2h). However, the suppression of SIRT1 and SIRT6 deacetylase activity with the selective inhibitors reduced the interaction between hnRNP A1 and the sirtuins (Fig. 2i). Therefore, glucose starvation upregulates SIRT1 and SIRT6 in HCC cells, enhances their interaction with hnRNP A1, and promotes the latter's deacetylation.

Four lysine sites of hnRNP A1 are deacetylated by SIRT1 and SIRT6

The PhosphoSitePlus database predicted 10 lysine (K) sites in hnRNP A1 that can be putatively acetylated (Fig. 3a). We mutated each of these sites to arginine (R) and tested the acetylation level of hnRNP A1 in the resulting KR mutants. Mutations in four sites (K3R, K52R, K87R, and K350R) significantly decreased the levels of acetylated hnRNP A1 (Fig. 3b). All the four sites were simultaneously mutated to form a deacetylated mimetic (4KR) of hnRNP A1, which had predictably lower acetylation levels than wild-type hnRNP A1, and did not respond any further to deacetylation even after the overexpression of SIRT1 and SIRT6, further indicating that the deacetylation of hnRNP A1 is dependent on these sirtuins (Fig. 3c). Inhibitors of SIRT1 and SIRT6 increased the acetylation level of hnRNP A1 but not of hnRNP A1 4KR (Fig. 3d). However, glucose starvation resulted in a similar reduction in acetylation levels of both hnRNP A1 and 4KR (Fig. 3e). co-IP assay showed a significant reduction in the interaction between hnRNP A1 4KR and SIRT1 (Fig. 3f) or SIRT6 (Fig. 3g). Taken together, the deacetylation of K3, K52, K87, and K350 is reduced during glucose starvation, and these residues are necessary for SIRT1- and SIRT6-mediated deacetylation of hnRNP A1.

Table 1 Correlation between hnRNP A1 expression and clinical data of HCC patients

		All cases	High hnRNP A1 expression	Low hnRNP A1 expression	*p* Value
Participants		78	52	26	
Sex	Male	66	44	22	1.000
	Female	12	8	4	
Age	<60 years	64	44	20	0.404
	≥60 years	14	8	6	
Tumor stage	I	4	1	3	0.021*
	II	24	12	12	
	III	47	36	11	
	IV	3	3	0	
Tumor metastasis	Y	8	5	3	0.792
	N	70	47	23	
Lymph node metastasis	Y	3	2	1	1.000
	N	75	50	25	
Tumor size	≤8 cm	54	32	22	0.037*
	>8 cm	24	20	4	

HCC hepatocellular carcinoma

*$p < 0.05$

Deacetylated hnRNP A1 inhibits glycolysis in HCC cells

Since hnRNP A1 is known to promote glycolysis by modulating the alternative splicing of PKM2 [25–28], we determined whether the acetylation or deacetylation of hnRNP A1 also affected glucose metabolism in HCC cells. Under normal high-glucose conditions, hnRNP A1 overexpression promoted glucose uptake in HepG2 and HuH-7 cells, while the deacetylated hnRNP A1 4KR mimetic reduced glucose uptake relative to hnRNP A1. However, there was no significant difference in the glucose uptake levels in HepG2 or HuH-7 cells overexpressing either hnRNP A1 or 4KR under glucose-starvation conditions (Fig. 4a). In addition, ^{18}F-fluorodeoxyglucose (^{18}F-FDG) uptake was enhanced in hnRNP A1-overexpressing and decreased in 4KR-expressing HCC cells at normal glucose levels, while it was unaffected by the hnRNP A1 status following glucose starvation (Fig. 4b). To reduce the interference of endogenous hnRNP A1 on the experimental results, we knocked down *hnRNP A1* with siRNA in HepG2 cells and then overexpressed hnRNP A1 or 4KR. The results showed that glucose uptake in 4KR-expressing cells was lower than that in hnRNP A1-expressing cells only under normal glucose culture conditions (Supplementary Fig. 3a and 3b). Similar kinetics of lactate (Fig. 4c, Supplementary Fig. 3c) and cytoplasmic pyruvate (Fig. 4d, Supplementary Fig. 3d) production were seen in the hnRNP A1/4KR cells vis-à-vis glucose concentration. Finally, the deacetylated 4KR mimetic resulted in a higher oxygen-consumption rate, an indicator of mitochondrial oxidative metabolism, compared to hnRNP A1 (Fig. 4e), but no significant difference was seen after glucose starvation (Fig. 4f). Taken together, our findings demonstrate that deacetylation of hnRNP A1 inhibits glycolysis and promotes mitochondrial metabolism in HCC cells.

Deacetylated hnRNP A1 blocks the alternative splicing of *PKM* mRNA to *PKM2*

HnRNP A1 enhances glucose metabolism by promoting the alternative splicing of the *PKM* mRNA to *PKM2*. In contrast, the deacetylation mimetic of hnRNP A1 increased the relative proportion of *PKM1* mRNA, which indicates that deacetylation of hnRNP A1 inhibited the generation of the *PKM2* isoform (Fig. 5a, Supplementary Fig. 4a). HnRNP A1 mediated the excision of exon 9 of the *PKM* pre-mRNA, which retained exon 10 and thus generated *PKM2* mRNA (Fig. 5b). Polymerase chain reaction (PCR) amplification of the fragment between exons 8 and 11 indicated that 4KR promoted the *PKM1* isoform as compared to the wild-type hnRNP A1 under high-glucose conditions (Fig. 5c, Supplementary Fig. 4b), but had no effect under glucose starvation (Fig. 5d). Compared with hnRNP A1, the 4KR mimetic also increased PKM1 protein levels under normal glucose conditions (Fig. 5e, Supplementary Fig. 4c). Previous studies have shown that hnRNP A1 binds to the intron sequence next to exon 9 (*EI9*) to facilitate the exclusion of *PKM* exon 9 [29]. We, therefore, established a 5'-biotin-labeled *EI9* sequence (19 bp), and RNA-affinity

Table 2 Correlation between the immunohistochemical staining intensity of several HCC biopsy markers and hnRNP A1 expression in HCC

		hnRNP A1 expression		*R* (*p* Value)
	Score	Low	High	
Hep-1	0	4	12	0.056 (0.352)
	1+	11	12	
	2+	6	12	
	3+	5	15	
HBsAg	0	7	12	0.175 (0.254)
	1+	14	20	
	2+	1	5	
	3+	3	15	
CK18	0	4	9	0.056 (0.352)
	1+	1	5	
	2+	10	15	
	3+	10	23	
CK19	0	25	45	0.000 (0.701)
	1+	1	5	
	2+	0	2	
	3+	0	0	
CD34	0	4	2	0.140 (0.206)
	1+	2	7	
	2+	6	8	
	3+	14	35	
β-Catenin	0	7	4	0.361 (0.025*)
	1+	1	10	
	2+	2	5	
	3+	0	0	
MUC-1	0	20	49	–0.227 (0.129)
	1+	2	1	
	2+	0	0	
	3+	1	0	
Glypican-3	0	14	19	0.232 (0.038*)
	1+	4	12	
	2+	4	3	
	3+	1	14	
P65	0	1	1	0.000 (0.919)
	1+	5	8	
	2+	1	1	
	3+	0	0	

HCC hepatocellular carcinoma

*$p < 0.05$

chromatography [11] showed that the biotinylated *EI9* RNA bound weakly to 4KR relative to hnRNP A1 under normal glucose conditions, while neither bound to *EI9* under glucose starvation (Fig. 5f). In addition, the activity of PK was significantly lower in 4KR HepG2 cells compared to the cells expressing hnRNP A1 (Fig. 5g), but only under normal and not low-glucose conditions (Fig. 5h). Taken together, deacetylation of hnRNP A1 promotes the alternative splicing of *PKM* mRNA to *PKM1* under normal glucose conditions, thereby inhibiting PK function in HCC cells.

Deacetylated hnRNP A1 suppresses PKM2-mediated β-catenin activation following glucose induction

Since PKM2 acts as a β-catenin coactivator to promote β-catenin-associated transcriptional activation [13], we next investigated the effect of hnRNP A1 deacetylation on this process. Under normal glucose conditions, the high expression of hnRNP A1 promoted the interaction between PKM2 and β-catenin, which was inhibited by the 4KR mimetic in HepG2 cells. However, no significant difference was seen during glucose starvation (Fig. 6a, b). PKM2 binding with β-catenin in the hnRNP A1 cells upregulated the downstream genes, including *GlutI*, *LDHA*, *PDK1*, *CCND1*, and *Myc*, while 4KR downregulated these genes in comparison with hnRNP A1 under normal conditions. The PKM2–β-catenin pathway was unaffected in the glucose-starved state (Fig. 6c, Supplementary Fig. 4d–h). Therefore, deacetylation of hnRNP A1 inhibits the binding between PKM2 and β-catenin, and inhibits the transcription of the downstream genes.

Deacetylated hnRNP A1 suppresses HCC growth in vitro and in vivo

We established HepG2 cell lines stably expressing either FLAG-hnRNP A1 or the 4KR mimetic. Deacetylation of hnRNP A1 inhibited HepG2 cell proliferation, as read by CCK-8 and colony-forming assays, under normal glucose but not low-glucose conditions (Fig. 7a, b). In addition, 4KR significantly inhibited in vivo HCC tumorigenesis (Fig. 7c) and significantly reduced the tumor volume (Fig. 7d) and weight (Supplementary Fig. 5a) compared to the hnRNP A1-overexpressing HCC cells. The ^{18}F-FDG positron emission tomography–computed tomography (PET/CT) results showed significantly reduced ^{18}F-FDG uptake in tumors expressing 4KR relative to hnRNP A1 (Fig. 7c). Compared to hnRNP A1, 4KR-expressing xenograft tumors showed higher levels of PKM1 and lower expression of PKM2 (Fig. 7e). Furthermore, the anti-proliferative effect of hnRNP A1 deacetylation was attributed to the regulation of SIRT1 and SIRT6. After the overexpression of SIRT1 and SIRT6 in HepG2 cells, the difference between hnRNP A1 and 4KR levels on cell proliferation was reduced (Fig. 7f). Xenograft tumor assays in vivo also confirmed that there was no significant difference in tumor growth between hnRNP A1 and 4KR after using the SIRT1 activator SRT1720 (Fig. 7g, h, Supplementary Fig. 5b). A PKM2-

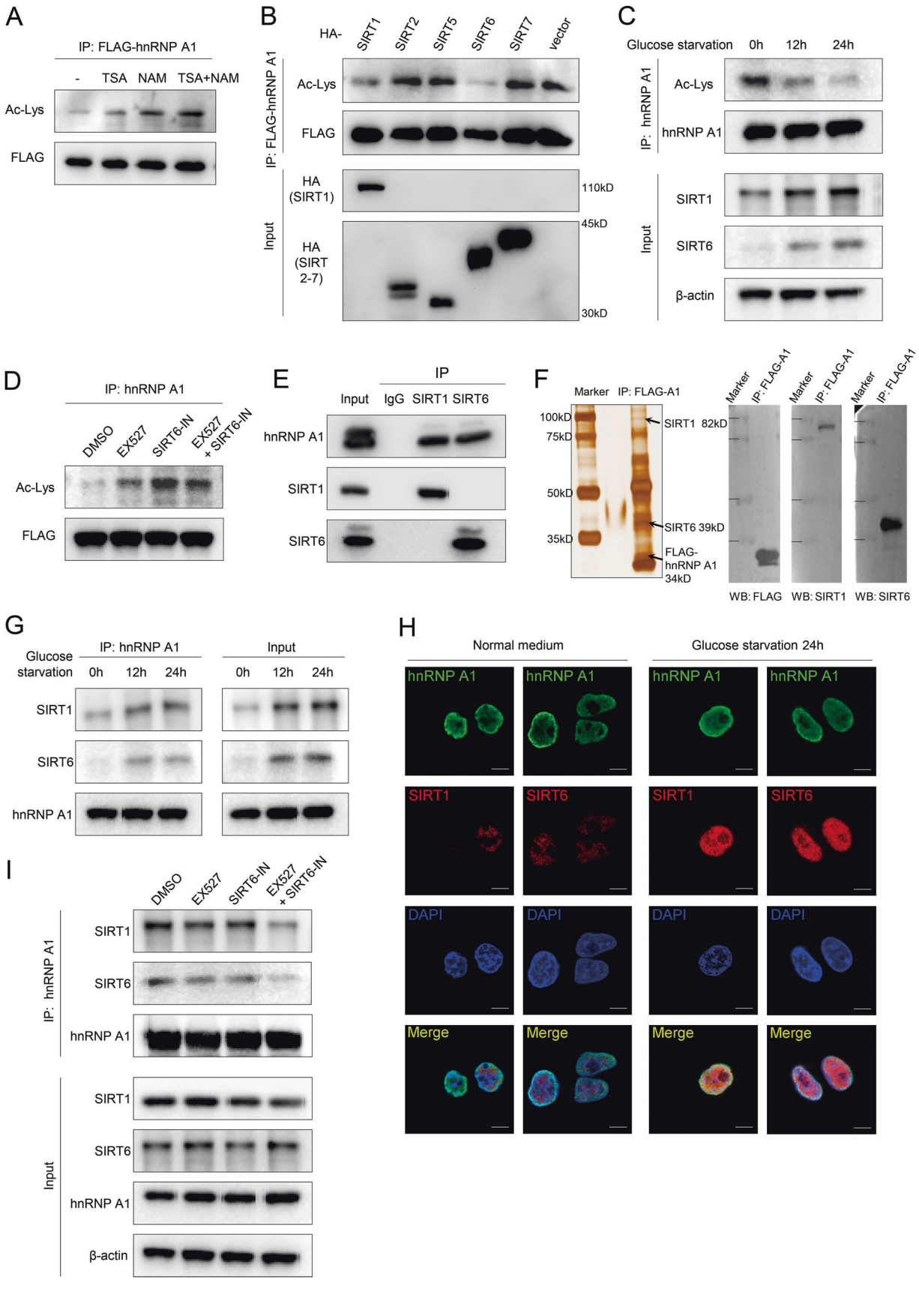
A
IP: FLAG-hnRNP A1
- TSA NAM TSA+NAM
Ac-Lys
FLAG
B
HA- SIRT1 SIRT2 SIRT5 SIRT6 SIRT7 vector
IP: FLAG-hnRNP A1
Ac-Lys
FLAG
Input
HA (SIRT1)
HA (SIRT 2-7)
110kD
45kD
30kD
C
Glucose starvation 0h 12h 24h
IP: hnRNP A1
Ac-Lys
hnRNP A1
Input
SIRT1
SIRT6
β-actin
D
IP: hnRNP A1
DMSO EX527 SIRT6-IN EX527 + SIRT6-IN
Ac-Lys
FLAG
E
Input IgG SIRT1 SIRT6
IP
hnRNP A1
SIRT1
SIRT6
F
Marker IP: FLAG-A1
100kD
75kD
50kD
35kD
SIRT1 82kD
SIRT6 39kD
FLAG-hnRNP A1 34kD
Marker IP: FLAG-A1
Marker IP: FLAG-A1
Marker IP: FLAG-A1
WB: FLAG WB: SIRT1 WB: SIRT6
G
Glucose starvation
IP: hnRNP A1
Input
0h 12h 24h 0h 12h 24h
SIRT1
SIRT6
hnRNP A1
H
Normal medium
Glucose starvation 24h
hnRNP A1
SIRT1
SIRT6
DAPI
Merge
I
DMSO EX527 SIRT6-IN EX527 + SIRT6-IN
IP: hnRNP A1
SIRT1
SIRT6
hnRNP A1
Input
SIRT1
SIRT6
hnRNP A1
β-actin

◀ **Fig. 2** HnRNP A1 was deacetylated by sirtuins and interacted with SIRT1 and SIRT6 in glucose-starved HCC cells. **a** FLAG-hnRNP A1-transfected HepG2 cells were treated with DMSO, 5 μM TSA, 10 mM NAM, or 5 μM TSA + 10 mM NAM for 24 h, followed by FLAG-hnRNP A1 immunoprecipitation and lysine-acetylation detection. **b** HepG2 cells overexpressing hnRNP A1 and HA-SIRT1, HA-SIRT2, HA-SIRT5, HA-SIRT6, HA-SIRT7 or the empty vector were lysed, followed by FLAG-hnRNP A1 immunoprecipitation and-lysine acetylation detection. **c** HepG2 cells were glucose starved for 0, 12, and 24 h, and the acetylated hnRNP A1 levels were detected. **d** HepG2 cells cultured under normal glucose conditions were treated with DMSO, 20 μM EX527, 100 μM SIRT6 inhibitor or 20 μM EX527 + 100 μM SIRT6 inhibitor for 24 h, and acetylated hnRNP A1 levels were detected. **e** HepG2 cell lysates were immunoprecipitated with anti-SIRT1 and anti-SIRT6 antibody or rabbit IgG, and immunoblotted with anti-hnRNP A1 antibody. **f** Lysates of HepG2 cells over-expressing FLAG-hnRNP A1 were immunoprecipitated with anti-FLAG antibody. Immunoprecipitated bands of FLAG-hnRNP A1, SIRT1, and SIRT6 were visualized by silver staining and western blotting. **g** HepG2 cells cultured in 5 mM glucose for 0, 12, and 24 h were lysed, and following hnRNP A1 immunoprecipitation, SIRT1 and SIRT6 were detected by western blotting. **h** In situ expression of hnRNP A1 (green), SIRT1 (red), and SIRT6 (red) in HepG2 cells was detected by immunofluorescence (scale bar, 10 μm). **i** HepG2 cells were treated with DMSO, 20 μM EX527, 100 μM SIRT6 inhibitor, or 20 μM EX527 + 100 μM SIRT6 inhibitor, and after hnRNP A1 immunoprecipitation, SIRT1 and SIRT6 were detected. DMSO, dimethyl sulfoxide; NAM, nicotinamide; TSA, trichostatin A

specific inhibitor (Compound 3K [30]) suppressed the proliferation of HepG2 cells expressing hnRNP A1 but not 4KR (Fig. 7i), which suggested that the promotion of proliferation by hnRNP A1 acetylation was dependent on PKM2. Taken together, under normal conditions, low levels of sirtuins put hnRNP A1 in an acetylated state, thereby upregulating PKM2 levels and activating glycolysis in HCC tumors. However, under glucose starvation, high levels of sirtuins promoted deacetylation of hnRNP A1, which inhibited PKM2-dependent glycolysis (Fig. 7j). Our data confirmed that the effect of deacetylated hnRNP A1 on tumor glycolysis was dependent on glucose levels.

Discussion

The alternative splicing of *PKM* pre-mRNA to *PKM2*, and the increase in its levels relative to *PKM1*, enhances anaerobic glycolysis and provides a selective advantage to the tumor cells. The alternative splicing of *PKM* is regulated by hnRNP A1, hnRNP A2/B1, and PTB [25, 31]. Post-transcriptional modifications of acetylated hnRNPs have been observed in tumors and other pathological conditions. In KRAS-mutated colorectal cancer, for example, hnRNP A1 acetylation is regulated by the epidermal growth factor [32]. Similarly, HnRNP A2/B1 is acetylated by acetyltransferase p300 and promotes the transcription of cyclooxygenase-2 to promote the growth of lung cancer cells [33]. Acetylation of the RNA-recognition motifs of PTB regulates its nuclear translocation and pre-mRNA splicing [34]. However, the role of post-transcriptional modification of hnRNPs in tumor growth and metabolism is not fully understood. We identified four lysine residues in hnRNP A1 that were deacetylated by SIRT1 and SIRT6 in HCC cells, resulting in the inhibition of *PKM2* alternative splicing and of glycolysis.

Tumor cells have evolved various mechanisms that help them adapt to hypoxia or nutrient-deficient microenvironments. Excessive glucose uptake is one of the hallmarks of tumor cells, which also causes hypoglycemia in cancer patients [35]. Glucose starvation alters the metabolic and cell-signaling pathways and modifies tumor cell proteins, mainly via the acetylation of histones or non-histones. During nutrient starvation, SIRT1 increases the activity of PGC1α and FOXO1 via deacetylation, and increases the expression of gluconeogenesis-related enzymes in the liver [36, 37]. Glucose starvation in A549 cells inhibited radiotherapy-induced histone acetylation, indicating that glucose deficiency can induce deacetylase activity [38]. In HCC cells, glucose starvation suppressed the activity of the tumor suppressor and acetyltransferase TIP60, which inhibited p53 acetylation thereby altering cell growth and apoptosis [39]. In addition, metabolic enzymes also undergo acetylation modifications following glucose induction. Previous studies have confirmed that a high concentration of glucose promoted the acetylation of PKM2, which stabilized the protein in the tumor cells and increased glucose metabolism and activated β-catenin-related signaling pathways [40, 41]. RNA alternative splicing is also a hallmark of tumors, and the acetylation or deacetylation of splicing factors, therefore, regulates tumor growth and metabolism. For example, glucose starvation enhanced the deacetylation of the RNA-splicing factor SRSF5 and inhibited lung cancer progression [42]. We found that acetylation of hnRNP A1, another RNA-splicing factor, is also regulated by glucose. Glucose starvation induced hnRNP A1 deacetylation by increasing the expression of SIRT1 and SIRT6, inhibiting PKM2-dependent glycolysis and tumorigenesis of HCC cells.

The inhibition of glycolysis by the deacetylated mimetic hnRNP A1 4KR was more pronounced under normal than under low-glucose conditions. Since deacetylase activity, including that of SIRT1 and SIRT6, is usually low under normal conditions (high glucose), a higher level of acetylated hnRNP A1 is seen in this state. Mutations in the four acetylation sites of hnRNP A1 markedly reduce its acetylation level and push *PKM* mRNA splicing towards *PKM1*, thereby inhibiting glycolysis and proliferation of HCC. As the levels of sirtuins increased with glucose starvation, the acetylation of hnRNP A1 was reduced and was close to that of the 4KR mutant. Therefore, hnRNP A1

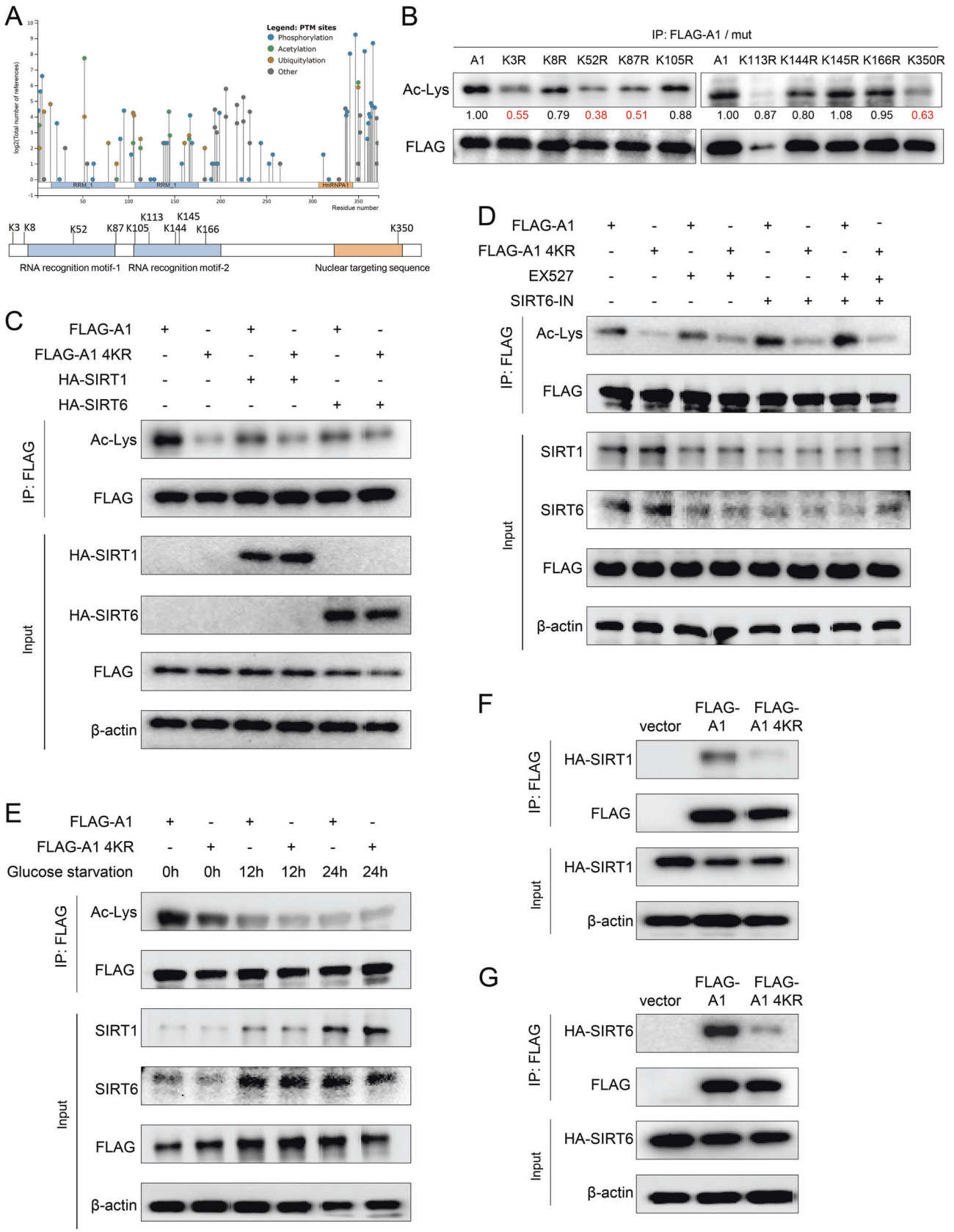
A
Legend: PTM sites
Phosphorylation
Acetylation
Ubiquitylation
Other
log2(Total number of references)
Residue number
RRM_1
RRM_1
HnRNPA1
K3 K8 K52 K87 K105 K113 K144 K145 K166 K350
RNA recognition motif-1
RNA recognition motif-2
Nuclear targeting sequence
B
IP: FLAG-A1 / mut
A1 K3R K8R K52R K87R K105R A1 K113R K144R K145R K166R K350R
Ac-Lys
1.00 0.55 0.79 0.38 0.51 0.88 1.00 0.87 0.80 1.08 0.95 0.63
FLAG
C
FLAG-A1
FLAG-A1 4KR
HA-SIRT1
HA-SIRT6
IP: FLAG
Ac-Lys
FLAG
Input
HA-SIRT1
HA-SIRT6
FLAG
β-actin
D
FLAG-A1
FLAG-A1 4KR
EX527
SIRT6-IN
IP: FLAG
Ac-Lys
FLAG
Input
SIRT1
SIRT6
FLAG
β-actin
E
FLAG-A1
FLAG-A1 4KR
Glucose starvation 0h 0h 12h 12h 24h 24h
IP: FLAG
Ac-Lys
FLAG
Input
SIRT1
SIRT6
FLAG
β-actin
F
vector
FLAG-A1
FLAG-A1 4KR
IP: FLAG
HA-SIRT1
FLAG
Input
HA-SIRT1
β-actin
G
vector
FLAG-A1
FLAG-A1 4KR
IP: FLAG
HA-SIRT6
FLAG
Input
HA-SIRT6
β-actin

◀ **Fig. 3** Four lysine residues (K3, K52, K87, and K350) of hnRNP A1 were deacetylated by SIRT1 and SIRT6. **a** PhosphoSitePlus database showed 10 putative lysine-acetylation sites in hnRNP A1, which are located in the RNA-recognition and nuclear-localization motifs. **b** The FLAG-tagged hnRNP A1 or A1-KR was transfected into HepG2 cells, and lysine acetylation levels were detected after immunoprecipitating the FLAG-tagged proteins. The relative acetylation levels were calculated by gray intensity analysis using Image J software. **c** FLAG-hnRNP A1 (or 4KR) and SIRT1 (or SIRT6) were transfected into HepG2 cells simultaneously, and the FLAG-hnRNP A1 (or 4KR) proteins were immunoprecipitated and probed for acetylation. **d** FLAG-hnRNP A1 (or 4KR)-transfected HepG2 cells were treated with DMSO, 20 μM EX527, 100 μM SIRT6 inhibitor, or 20 μM EX527 + 100 μM SIRT6 inhibitor for 24 h, and the acetylation of FLAG-hnRNP A1 (or 4KR) protein was detected. **e** FLAG-hnRNP A1 (or 4KR)-transfected HepG2 cells were glucose starved for 0, 12, and 24 h, and the acetylation of FLAG-hnRNP A1 (or 4KR) was detected. **f, g** HepG2 cells transfected with FLAG-hnRNP A1 (or 4KR) and HA-SIRT1 (or HA-SIRT6) were lysed, and the bound HA-SIRT1 (or HA-SIRT6) protein levels were detected after FLAG-hnRNP A1 (or 4KR) immunoprecipitation. DMSO, dimethyl sulfoxide

had little effect on glycolysis under glucose starvation. In fact, in glucose- and energy-deficient conditions, tumor cells show enhanced deacetylase activity to reduce glycolysis and increase mitochondrial oxidation [43]. On one hand, energy-deficient tumor microenvironment promoted the expression of deacetylase such as SIRT6 and directly reduced the acetylation status of PKM2, thereby reprogramming metabolism [21]. On the other hand, the lack of energy reduced the acetylation level of hnRNP A1, which in turn reduced the production of PKM2, and thus, the expression of PKM2 and its post-transcriptional modifications were also suppressed (Supplementary Fig. 5c). Based on our findings, we propose a metabolic adaptive mechanism in HCC cells facing insufficient energy supply.

Materials and methods

Cell lines and culture conditions

HepG2, HuH-7, and 293T cell lines were purchased from ATCC and cultured in high-glucose Dulbecco's modified Eagle's medium (DMEM) (25 mM D-glucose; Gibco, Waltham, MA, USA) supplemented with 10% fetal bovine serum (Gibco), 100 mg/ml penicillin, and 100 mg/ml streptomycin sulfate (Gibco) at 37 °C under 5% CO_2. For glucose starvation, cells were cultured with the normal medium for 24 h, and then replaced with glucose-free DMEM (Gibco) containing 5 mM D-glucose and 10% fetal bovine serum. All cell lines were authenticated by short tandem repeats (STR) profiling and mycoplasma was tested every 2 weeks.

Plasmids and reagents

Human hnRNP A1, hnRNP A1 4KR, SIRT1, SIRT2, SIRT5, SIRT6, and SIRT7 sequences were cloned into pcDNA4TO-Flag/HA vectors. For lentiviral construction, hnRNP A1 and hnRNP A1 4KR were cloned into pLenti-CMV-EGFP-3FLAG-Puro vectors and stably expressed in HepG2 cells. Lipofectamine 2000 was purchased from Invitrogen (Waltham, MA, USA), TSA and NAM from Sigma-Aldrich (St. Louis, MO, USA), and EX527, SIRT6 inhibitor, and PKM2 inhibitor from Selleck Chemicals (Shanghai, China). The following primary antibodies were used: anti-FLAG (Sigma), anti-HA (Abmart, Shanghai, China), anti-hnRNP A1 (Abcam, Cambridge, UK), anti-SIRT1 and anti-SIRT6 (Proteintech, Wuhan, China), anti-acetylated lysine, anti-PKM2, anti-PKM2 pY105, anti-PKM1, anti-β-catenin and anti-β-actin (all from Cell Signaling Technology, Danvers, MA, US).

Immunohistochemistry

Tissue samples were surgically resected from consenting patients at Ren Ji Hospital, Shanghai Jiao Tong University School of Medicine. All experimental procedures were approved by the Human Ethics Committee of Shanghai University of Medicine and Health Sciences. Tissue sections were treated with 3% H_2O_2 to block endogenous peroxidase activity and then incubated with anti-hnRNP A1 (1:500). Following incubation with HRP-conjugated secondary antibody, the positive signals were visualized by diaminobenzidine chromogen. Two independent researchers scored hnRNP A1 staining on the basis of distribution and intensity. The percentage of stained cells was scored as 0 (0–5%), 1 (5–25%), 2 (25–50%), and 3 (50–100%), and the staining intensities were scored as 0 (no staining), 1 (weak), 2 (medium), and 3 (strong). The expression of hnRNP A1 in each sample was calculated by multiplying the percentage scores with the staining intensity scores. Samples were then classified as high expressing (score ≥ 6) or low expressing (score < 6).

Co-immunoprecipitation and lysine-acetylation assay

For exogenous co-IP, FLAG-hnRNP A1- and HA-SIRT1 (or SIRT6)-overexpressing cells were lysed with radioimmunoprecipitation assay (RIPA) buffer. The cell extracts were incubated overnight with anti-FLAG beads (Sigma) at 4 °C. After washing three times with immunoprecipitation buffer, the samples were analyzed by western blotting using antibodies against HA-SIRT1 (or SIRT6). For endogenous

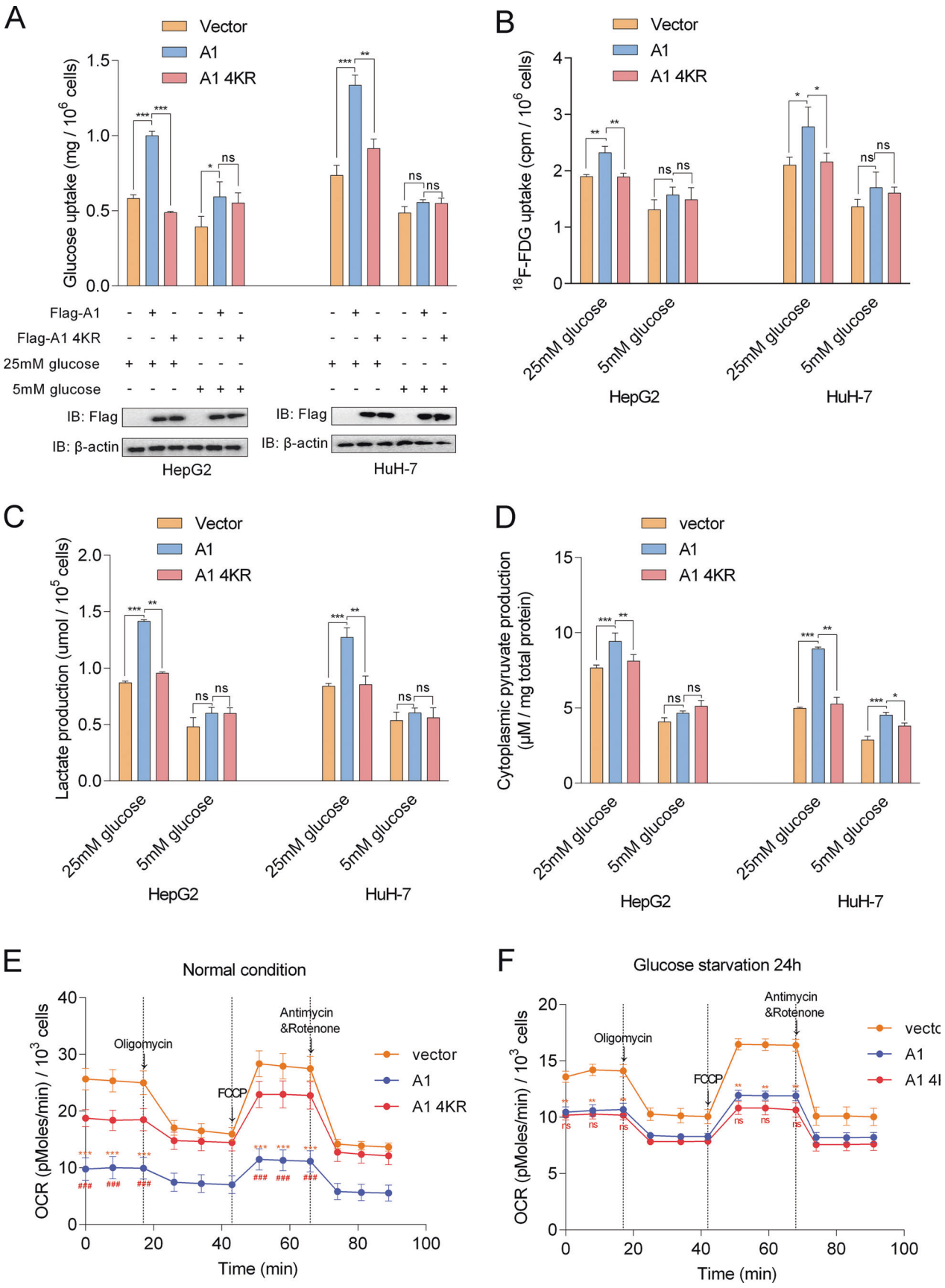
A
Vector
A1
A1 4KR
Glucose uptake (mg / 10^6 cells)
Flag-A1
Flag-A1 4KR
25mM glucose
5mM glucose
IB: Flag
IB: β-actin
HepG2
HuH-7
B
18F-FDG uptake (cpm / 10^6 cells)
25mM glucose
5mM glucose
HepG2
HuH-7
C
Lactate production (umol / 10^5 cells)
D
vector
Cytoplasmic pyruvate production (μM / mg total protein)
E
Normal condition
OCR (pMoles/min) / 10^3 cells
Oligomycin
FCCP
Antimycin &Rotenone
Time (min)
F
Glucose starvation 24h

◀ **Fig. 4** Deacetylated hnRNP A1 inhibited glycolysis and increased aerobic metabolism in HCC cells. **a** HepG2 and HuH-7 cells transfected with empty vector, FLAG-hnRNP A1 or 4KR were cultured for 24 h under normal (25 mM) or low-glucose (5 mM) conditions, and then in a suitable medium for glucose-uptake assays. The expression of FLAG-hnRNP A1 and 4KR proteins in the corresponding cells was analyzed by western blotting. **b** The above treated cells were incubated in PBS containing 4μCi/ml ^{18}F-FDG for 1 h, and ^{18}F-FDG uptake was measured by a gamma counter. **c** The above treated cells were incubated in a serum-free medium to detect lactate production. **d** The cells were lysed and the cytoplasmic levels of pyruvate were detected. **e, f** HepG2 cells expressing empty vector, FLAG-hnRNP A1, or 4KR were cultured for 24 h under normal (**e**) or low-glucose (**f**) conditions, and 10,000 cells of each were transferred to Seahorse XF24 cell-culture microplates to detect O_2 consumption. *$p < 0.05$, **$p < 0.01$, ***$p < 0.001$; ns, no significance. ^{18}F-FDGF, fluorodeoxyglucose; HCC, hepatocellular carcinoma; PBS, phosphate-buffered saline

co-IP, cell extracts were incubated overnight with anti-hnRNP A1 antibody (IgG as control), followed by 3 h with protein A/G (Pierce; Thermo Fisher Scientific, Waltham, MA, USA) at 4 °C, and analyzed for SIRT1 or SIRT6 expression by western blotting. For lysine-acetylation assay, immunoprecipitation with anti-FLAG or anti-hnRNP A1 antibodies was followed by western blotting against acetylated lysine-PKM2.

Immunofluorescence

HepG2 cells were cultured in 20 mm glass-bottomed culture dishes (NEST, Wuxi, China) in normal or glucose-starved conditions for 24 h. Attached cells were fixed with 4% paraformaldehyde in phosphate-buffered saline and then permeabilized with 0.25% Triton X-100. After treating the cells with blocking buffer (Beyotime, Shanghai, China) for 30 min, they were incubated overnight with anti-hnRNP A1, anti-SIRT1, and anti-SIRT6 at 4 °C, and then with the suitable secondary antibodies (anti-mouse-GFP and anti-rabbit-Cheery) for 1 h at room temperature. Following 4′,6-diamidino-2-phenylindole counterstaining, an anti-fluorescence quencher was added dropwise and fixed with a coverslip. Images were taken using a Nikon A1 + confocal microscope.

Glucose/^{18}F-FDG uptake and lactate production

HepG2 and HuH-7 cells transfected with FLAG-hnRNP A1 or 4KR were seeded in 12-well plates and incubated for 24 h under normal or glucose-starved conditions. For glucose-uptake and lactate-production assays, the culture medium was replaced with 500 μl serum-free high-glucose DMEM and collected after 6 h of incubation. The glucose and lactate levels of the samples were measured using glucose assay kit (Sigma) and lactate assay kit (Sigma) respectively. For the ^{18}F-FDG-uptake assay, the culture medium was replaced with 4 μCi/ml ^{18}F-FDG in phosphate-buffered saline, and the cells were incubated for 1 h at 37 °C. After lysing the cells with 1 M NaOH, the amount of ^{18}F-FDG uptake by the cells was measured using a gamma counter. All data were normalized by cell numbers.

Cytoplasmic pyruvate and pyruvate kinase assay

HepG2 and HuH-7 cells transfected with FLAG-hnRNP A1 or 4KR were seeded in 12-well plates and incubated for 24 h under normal or glucose-starved conditions. The cells were lysed with RIPA buffer, and the pyruvate levels or PK activity in the cell lysates was measured by the pyruvate assay kit (Sigma, MAK071) or PK assay kit (Sigma, MAK072), respectively, according to the manufacturer's instructions. Data were normalized to the total protein content, as measured by the BCA kit (Yeasen, Shanghai, China).

Cellular oxygen consumption assay

The cellular oxygen consumption was measured using the Seahorse XF24 Extracellular Flux Analyzer, which reflects the levels of mitochondrial respiration in the cells. Suitably treated HepG2 cells were seeded at the density of 1×10^4 cells/well in XF24 cell culture plates (Seahorse Bioscience, Agilent, USA) and incubated for 24 h under normal or glucose-starved conditions. The cells were then equilibrated in a CO_2 incubator at 37 °C for 60 min in low-buffer DMEM (Gibco) without bicarbonate before XF24 analysis. The respiratory chain inhibitors or activators (1 μM oligomycin, 1 μM carbonyl cyanide p-trifluoromethoxyphenylhydrazone (FCCP), 1 μM antimycin and rotenone, all from Sigma) were automatically injected into the microplate from the reagent port at the indicated times.

RNA-splicing assay

HepG2 and HuH-7 cells expressing hnRNP A1 or 4KR were cultured under normal and low-glucose conditions. RNA was extracted and then reverse transcribed into cDNA, and 28 cycles of semi-quantitative PCR were carried out using the following primers: e8-F(CTGAAGGCAGTGATGTGGCC) and e11-R(ACCCGGAGGTCCACGTCCTC). The PCR products (20 μl) were digested with PstI (New England Biolabs, USA) for 1 h, and the relative levels of *PKM1* and *PKM2* were analyzed by electrophoresis.

RNA-affinity purification

The RNA-affinity assay was performed as described in previous studies [11, 44]. Briefly, 1 nM of the synthetic single-stranded *EI9* RNA (5'-biotin-AGGUAGGGCC-CUAAGGGCA-3') and 100 μl Streptavidin–Agarose

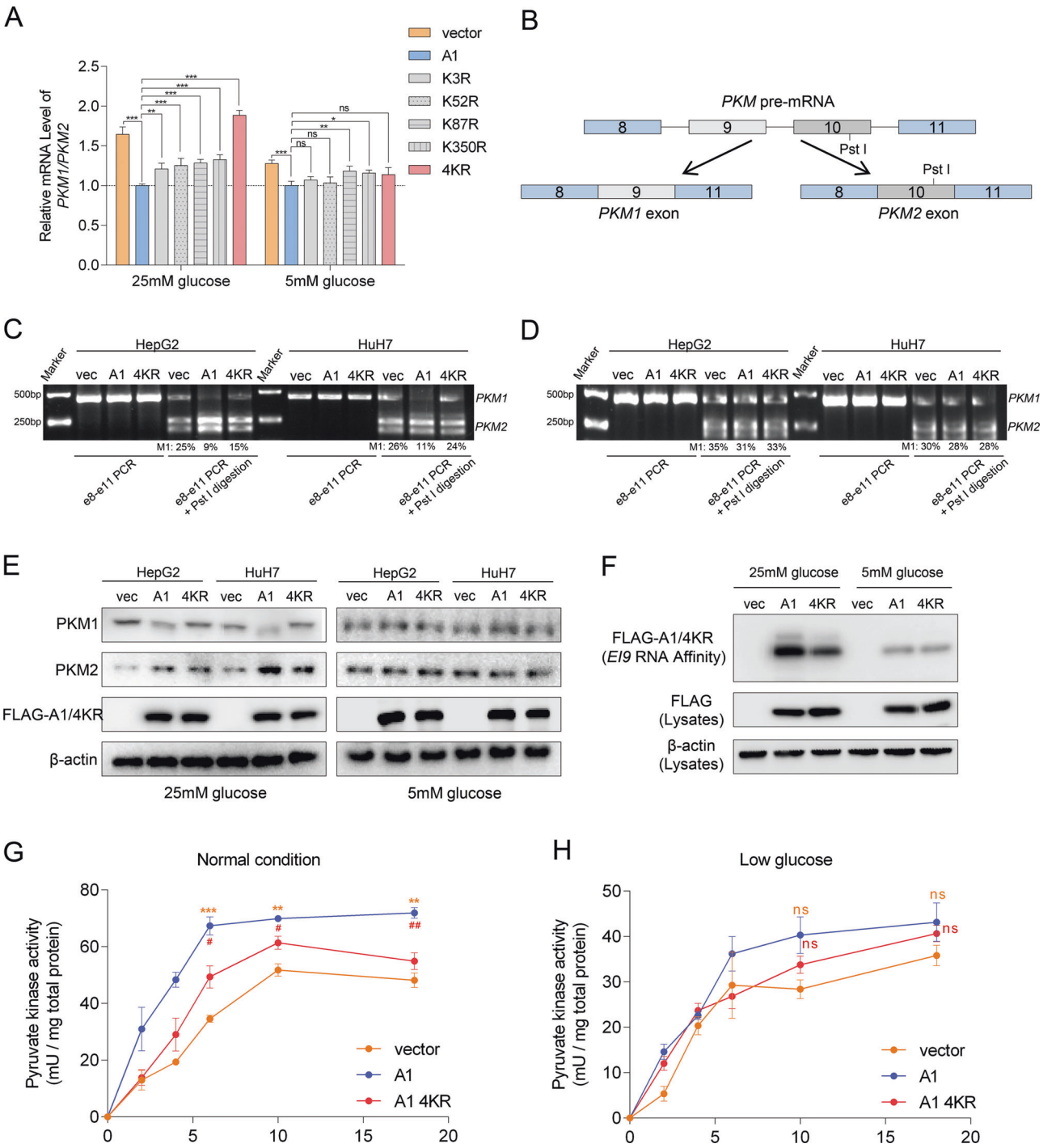

Fig. 5 Deacetylated hnRNP A1 decreased PKM2 and increased PKM1 levels in HCC cells by the alternate splicing of *PKM* mRNA. **a** The *PKM1* and *PKM2* mRNA levels in HepG2 expressing each A1 mutant under 25 or 5 mM glucose for 24 h were measured by RT-PCR. **b** Alternative splicing of *PKM* mRNA into *PKM1* and *PKM2* was detected by PstI digestion, which specifically targeted exon 10 of *PKM2*. **c, d** HepG2 and HuH-7 cells expressing the empty vector, FLAG-hnRNP A1 or 4KR, were grown under normal (**c**) or low-glucose (**d**) conditions, and exon 8 to exon 11 region of *PKM* was amplified by PCR, followed by the detection of the relative amount of *PKM1* and PstI-digested *PKM2*. **e** The levels of PKM1 and PKM2 proteins in HepG2 and HuH-7 cells were detected by respective antibodies. **f** The lysates of the HepG2 cells above were affinity purified using streptavidin–biotin-labeled *EI9* RNA agarose, and the bound proteins were detected using anti-FLAG antibody. **g, h** The activity of pyruvate kinase in the lysates of HepG2 cells cultured under normal (**g**) and low-glucose (**h**) conditions was suitably detected. $*p < 0.05$, $**p < 0.01$, $***p < 0.001$; ns, no significance. HCC, hepatocellular carcinoma; RT-PCR, real time-polymerase chain reaction

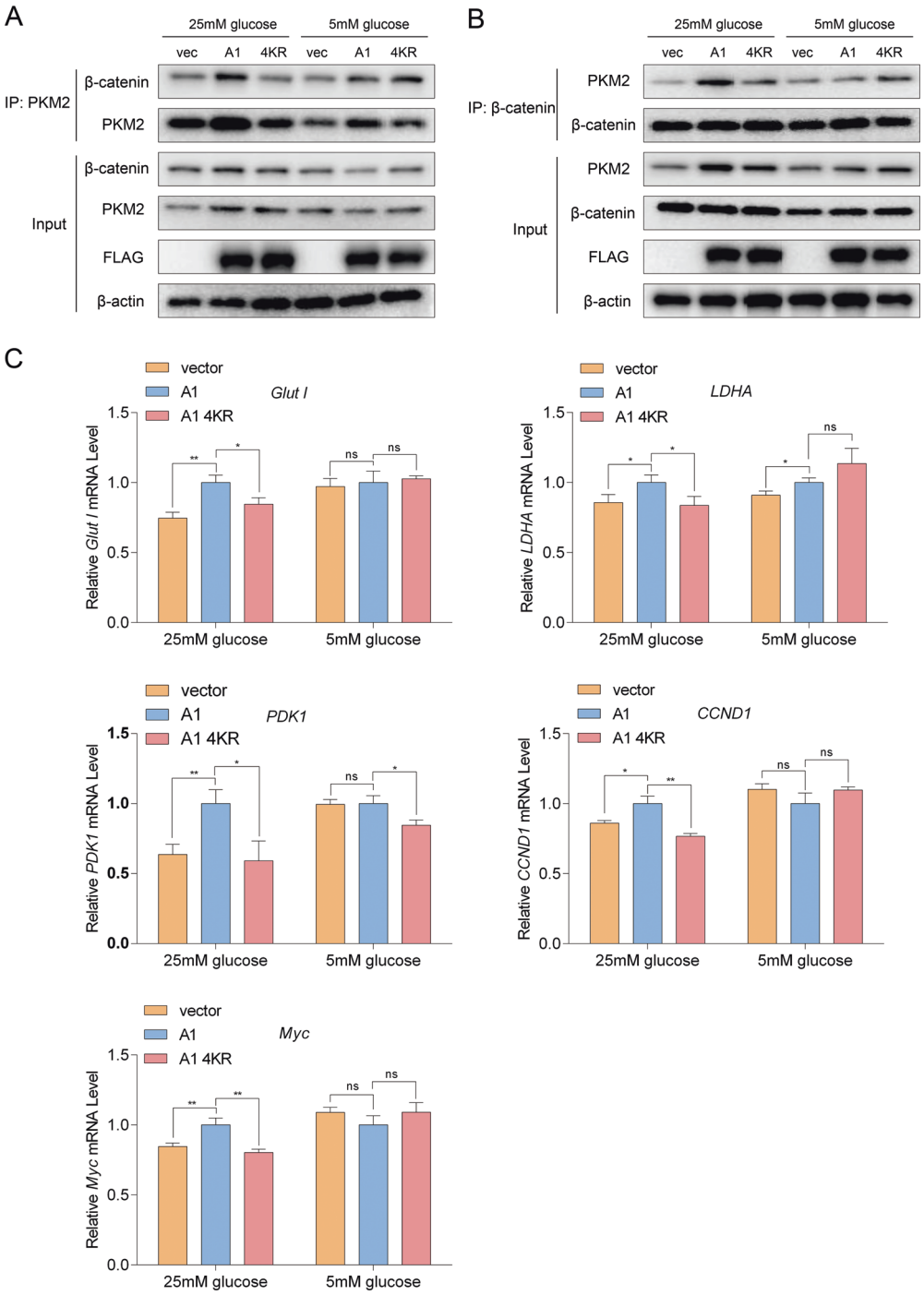

Fig. 6 Deacetylated hnRNP A1 suppressed PKM2-mediated β-catenin transcriptional activation under glucose induction in HCC cells. **a, b** HEPG2 cells expressing the empty vector, Flag-hnRNP A1 or 4KR, were cultured under normal or low-glucose conditions, and after immunoprecipitating PKM2 (**a**) or β-catenin (**b**) from the cell lysates, the bound β-catenin and PKM2 protein levels were detected. **c** *GlutI*, *LDHA*, *PDK1*, *CCND1*, and *Myc* mRNA levels were detected by RT-PCR in the above HepG2 cells. $*p < 0.05$, $**p < 0.01$, $***p < 0.001$; ns, no significance. HCC, hepatocellular carcinoma; RT-PCR, real time-polymerase chain reaction

(Sigma) were mixed with 500 µl RIPA buffer, and incubated overnight at 4 °C. The unbound agarose was removed by washing twice with RIPA buffer. HepG2 cells expressing hnRNP A1 or A1 4KR and cultured under normal or low-glucose conditions for 24 h were lysed, and the lysates were incubated with the biotin–RNA–agarose for 30 min at 30 °C. The expression of the RNA-binding proteins was then detected by western blotting.

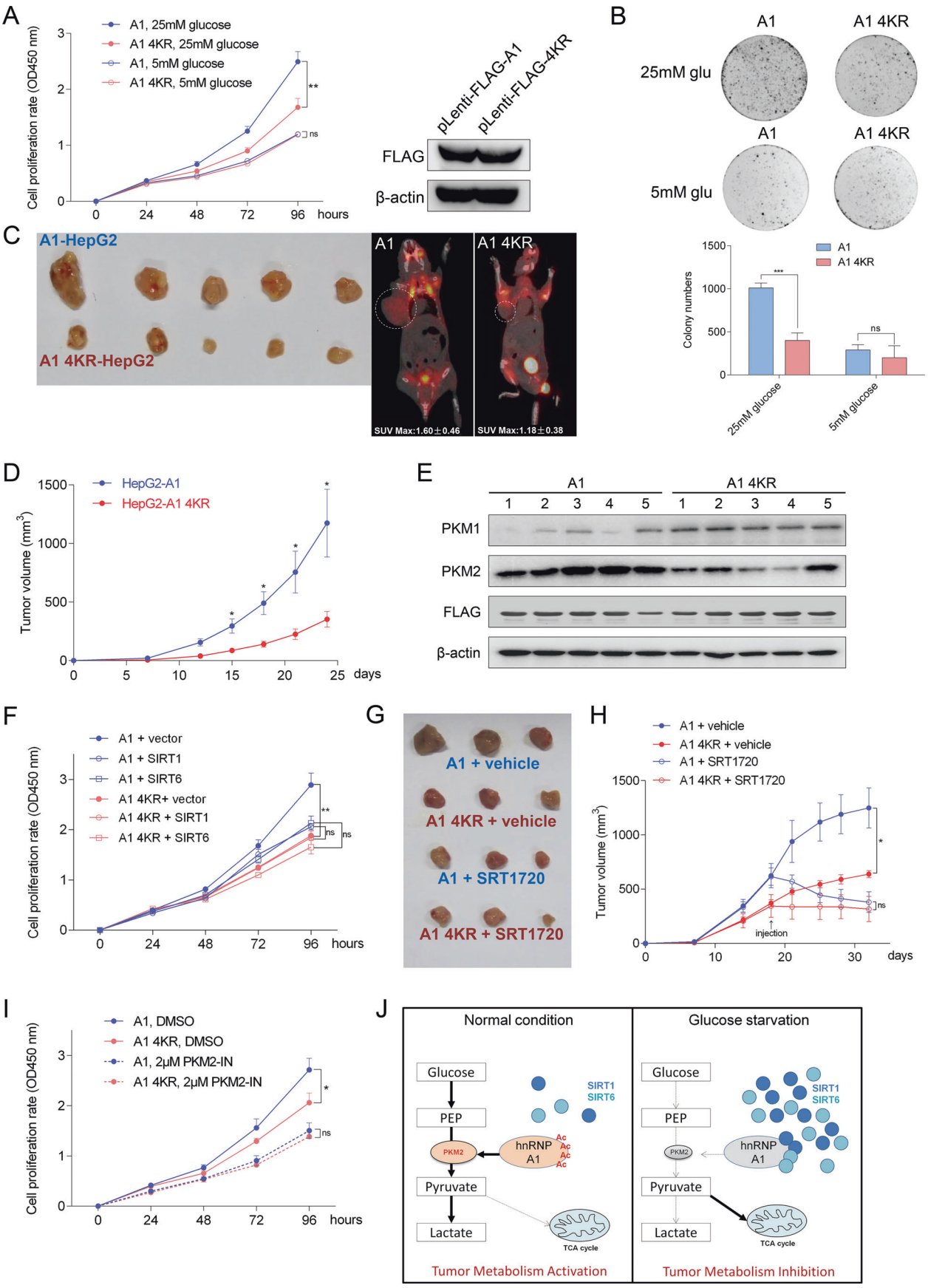
A
A1, 25mM glucose
A1 4KR, 25mM glucose
A1, 5mM glucose
A1 4KR, 5mM glucose
Cell proliferation rate (OD450 nm)
hours
pLenti-FLAG-A1
pLenti-FLAG-4KR
FLAG
β-actin
B
A1
A1 4KR
25mM glu
5mM glu
Colony numbers
25mM glucose
5mM glucose
C
A1-HepG2
A1 4KR-HepG2
SUV Max:1.60±0.46
SUV Max:1.18±0.38
D
HepG2-A1
HepG2-A1 4KR
Tumor volume (mm3)
days
E
PKM1
PKM2
F
A1 + vector
A1 + SIRT1
A1 + SIRT6
A1 4KR+ vector
A1 4KR + SIRT1
A1 4KR + SIRT6
G
A1 + vehicle
A1 4KR + vehicle
A1 + SRT1720
A1 4KR + SRT1720
H
A1 + vehicle
A1 4KR + vehicle
A1 + SRT1720
A1 4KR + SRT1720
injection
I
A1, DMSO
A1 4KR, DMSO
A1, 2μM PKM2-IN
A1 4KR, 2μM PKM2-IN
J
Normal condition
Glucose starvation
Glucose
PEP
PKM2
Pyruvate
Lactate
hnRNP A1
SIRT1
SIRT6
TCA cycle
Tumor Metabolism Activation
Tumor Metabolism Inhibition

◀ **Fig. 7** Deacetylated hnRNP A1 suppressed PKM2-mediated glycolysis and HCC growth through SIRT1 and SIRT6. **a** PLenti-Flag-hnRNP A1 and pLenti-Flag-4KR plasmids were stably infected into HepG2 cells. The same number of cells were plated in 96-well plates and cultured under normal or low-glucose conditions, and the number and viability of cells were measured every day by CCK-8 assay. **b** Colony-formation assay was performed with HepG2 cells treated as described above. **c** Representative PET/CT images of xenograft tumors induced in nude mice by hnRNP A1- or 4KR-expressing HepG2 cells, with the circled area representing the tumor site. **d** Changes in tumor volume during the experimental period. **e** The expression of PKM1 and PKM2 in xenograft tumors expressing hnRNP A1 or 4KR was detected. **f** HepG2 cells stably expressing hnRNP A1 and 4KR were transfected with the empty vector, HA-SIRT1 or HA-SIRT6, and CCK-8 proliferation assay was performed. **g**, **h** The cells expressing hnRNP A1 or 4KR were implanted subcutaneously in nude mice, and the SIRT1 agonist SRT1720 or the control vehicle was injected from the 18th day. After 2 weeks of treatment, the tumor was imaged (**g**) and the tumor volume was measured (**h**). **i** HepG2 cells stably expressing hnRNP A1 and 4KR were treated with DMSO or PKM2 inhibitor, followed by CCK-8 assay. **j** Expression pattern of different sirtuins and acetylation states of hnRNP A1 under different extracellular conditions. DMSO, dimethyl sulfoxide; HCC, hepatocellular carcinoma; PET/CT, positron emission tomography–computed tomography

Cell-proliferation assay

HepG2 cells stably expressing hnRNP A1 or 4KR were seeded in 96-well plates at a density of 1×10^4 cells/well. After 24 h, 10 µl CCK-8 solution (Dojindo, Kumamoto, Japan) was added to the medium, and the proliferation was quantified by measuring the absorbance at 450 nm. For the colony-formation assay, 200 suitably treated HepG2 cells were suspended in each well of a 12-well plate and cultured in high- or low-glucose medium. After 3 weeks, the cells were stained with 0.1% crystal violet, imaged, and the number of colonies was counted.

Xenograft tumor model and imaging

All animal experiments were performed in accordance with the guidelines provided by the Animal Ethics Committee of the Shanghai University of Medicine and Health Sciences. Five randomly selected 4-week-old male BALB/c SCID mice (Shanghai Laboratory Animal Center) were each inoculated subcutaneously with 5×10^6 HepG2 cells stably expressing hnRNP A1 or 4KR; no blinding of groups was done. Tumor sizes were measured over 24 days, and the results were expressed as the mean ± SD. Glucose uptake in the tumor xenografts was monitored by ^{18}F-FDG micro-PET/CT. The tumors were also scanned using Super Nova Micro-PET/CT scanner (Pingseng Healthcare, Suzhou, Shanghai) after injecting them intravenously with 200 µl saline containing 200 µCi ^{18}F-FDG. The standardized uptake value of the region of interest was then evaluated manually. In experiments in which SIRT1 agonists affected tumorigenesis, SRT1720 (Selleck Chemicals, Shanghai, China) was first configured with dimethyl sulfoxide to a stock solution of 30 mg/ml. Three nude mice per group were intravenously injected with 20 mg/kg SRT1720 (diluted in isotonic saline) three times a week after tumor formation for 18 days. As a control vehicle, 0.2% dimethyl sulfoxide in isotonic saline was administered intravenously. At the end of the experiment, the mice were sacrificed and tumors were photographed and weighed.

Statistical analysis

All data were statistically analyzed using Graphpad Prism 6 or SPSS 20 software. One-way analysis of variance and *t* test were used to analyze the variance between the two groups, and Pearson's test was used to determine the correlation between the two variables. Kaplan–Meier test was used for survival analysis. Data are presented as the mean ± SEM or SD of at least three independent experiments, and $p < 0.05$ was considered significant.

Acknowledgements This work was supported by research grants from the National Natural Science Foundation of China (Nos. 81530053, 81830052, 81771858, 81602415, 81670573, 81572719, 81874202, and 81803581) and Shanghai Municipal Education Commission (Class II Plateau Disciplinary Construction Program for Medical Technology of SUMHS, 2018–2020).

Compliance with ethical standards

Conflict of interest The authors declare that they have no conflict of interest.

References

1. Iansante V, Choy PM, Fung SW, Liu Y, Chai JG, Dyson J, et al. PARP14 promotes the Warburg effect in hepatocellular carcinoma by inhibiting JNK1-dependent PKM2 phosphorylation and activation. Nat Commun. 2015;6:7882.
2. Mazurek S. Pyruvate kinase type M2: a key regulator of the metabolic budget system in tumor cells. Int J Biochem Cell Biol. 2011;43:969–80.
3. Zhang LF, Lou JT, Lu MH, Gao C, Zhao S, Li B, et al. Suppression of miR-199a maturation by HuR is crucial for hypoxia-induced glycolytic switch in hepatocellular carcinoma. EMBO J. 2015;34:2671–85.
4. Williams AL, Khadka V, Tang M, Avelar A, Schunke KJ, Menor M, et al. HIF1 mediates a switch in pyruvate kinase isoforms after myocardial infarction. Physiol Genomics. 2018;50:479–94.
5. Chen H, Hewison M, Hu B, Adams JS. Heterogeneous nuclear ribonucleoprotein (hnRNP) binding to hormone response elements: a cause of vitamin D resistance. Proc Natl Acad Sci USA. 2003;100:6109–14.
6. Chettouh H, Fartoux L, Aoudjehane L, Wendum D, Claperon A, Chretien Y, et al. Mitogenic insulin receptor-A is overexpressed in

human hepatocellular carcinoma due to EGFR-mediated dysregulation of RNA splicing factors. Cancer Res. 2013;73:3974–86.
7. Park WC, Kim HR, Kang DB, Ryu JS, Choi KH, Lee GO, et al. Comparative expression patterns and diagnostic efficacies of SR splicing factors and HNRNPA1 in gastric and colorectal cancer. BMC Cancer. 2016;16:358.
8. Kim YJ, Kim BR, Ryu JS, Lee GO, Kim HR, Choi KH, et al. HNRNPA1, a splicing regulator, is an effective target protein for cervical cancer detection: comparison with conventional tumor markers. Int J Gynecol Cancer. 2017;27:326–31.
9. Roy R, Huang Y, Seckl MJ, Pardo OE. Emerging roles of hnRNPA1 in modulating malignant transformation. Wiley Interdiscip Rev RNA. 2017;8:e1431.
10. Chen M, Zhang J, Manley JL. Turning on a fuel switch of cancer: hnRNP proteins regulate alternative splicing of pyruvate kinase mRNA. Cancer Res. 2010;70:8977–80.
11. Huang JZ, Chen M, Chen, Gao XC, Zhu S, Huang H, et al. A peptide encoded by a putative lncRNA HOXB-AS3 suppresses colon cancer growth. Mol Cell. 2017;68:171–84.
12. Yang W, Zheng Y, Xia Y, Ji H, Chen X, Guo F, et al. ERK1/2-dependent phosphorylation and nuclear translocation of PKM2 promotes the Warburg effect. Nat Cell Biol. 2012; 14:1295–304.
13. Yang W, Xia Y, Ji H, Zheng Y, Liang J, Huang W, et al. Nuclear PKM2 regulates beta-catenin transactivation upon EGFR activation. Nature. 2011;480:118–22.
14. Dayton TL, Gocheva V, Miller KM, Bhutkar A, Lewis CA, Bronson RT, et al. Isoform-specific deletion of PKM2 constrains tumor initiation in a mouse model of soft tissue sarcoma. Cancer Metab. 2018;6:6.
15. Xu Q, Liu LZ, Yin Y, He J, Li Q, Qian X, et al. Regulatory circuit of PKM2/NF-kappaB/miR-148a/152-modulated tumor angiogenesis and cancer progression. Oncogene. 2015;34:5482–93.
16. Chen J, Chan AW, To KF, Chen W, Zhang Z, Ren J, et al. SIRT2 overexpression in hepatocellular carcinoma mediates epithelial to mesenchymal transition by protein kinase B/glycogen synthase kinase-3beta/beta-catenin signaling. Hepatology. 2013;57: 2287–98.
17. Zhang ZY, Hong D, Nam SH, Kim JM, Paik YH, Joh JW, et al. SIRT1 regulates oncogenesis via a mutant p53-dependent pathway in hepatocellular carcinoma. J Hepatol. 2015;62:121–30.
18. Ong ALC, Ramasamy TS. Role of Sirtuin1-p53 regulatory axis in aging, cancer and cellular reprogramming. Ageing Res Rev. 2018;43:64–80.
19. Agerholm M, Dall M, Jensen BAH, Prats C, Madsen S, Basse AL, et al. Perturbations of NAD(+) salvage systems impact mitochondrial function and energy homeostasis in mouse myoblasts and intact skeletal muscle. Am J Physiol Endocrinol Metab. 2018;314:E377–e95.
20. Park SH, Ozden O, Liu G, Song HY, Zhu Y, Yan Y, et al. SIRT2-mediated deacetylation and tetramerization of pyruvate kinase directs glycolysis and tumor growth. Cancer Res. 2016; 76:3802–12.
21. Bhardwaj A, Das S. SIRT6 deacetylates PKM2 to suppress its nuclear localization and oncogenic functions. Proc Natl Acad Sci USA. 2016;113:E538–47.
22. Zhu Y, Yan Y, Principe DR, Zou X, Vassilopoulos A. Gius D. SIRT3 and SIRT4 are mitochondrial tumor suppressor proteins that connect mitochondrial metabolism and carcinogenesis. Cancer Metab. 2014;2:15.
23. Chang C, Hua S, Zhang D, Wang Y, Shen Q, Bo L, et al. AMPK-dependent phosphorylation of GAPDH triggers Sirt1 activation and is necessary for autophagy upon glucose starvation. Mol Cell. 2015;60:930–40.
24. Parenti MD, Grozio A, Bauer I, Galeno L, Damonte P, Millo E, et al. Discovery of novel and selective SIRT6 inhibitors. J Med Chem. 2014;57:4796–804.
25. Clower CV, Chatterjee D, Wang Z, Cantley LC, Vander Heiden MG, Krainer AR. The alternative splicing repressors hnRNP A1/A2 and PTB influence pyruvate kinase isoform expression and cell metabolism. Proc Natl Acad Sci USA. 2010;107:1894–9.
26. Sun Y, Luo M, Chang G, Ren W, Wu K, Li X, et al. Phosphorylation of Ser6 in hnRNPA1 by S6K2 regulates glucose metabolism and cell growth in colorectal cancer. Oncol Lett. 2017;14:7323–31.
27. Luan W, Wang Y, Chen X, Shi Y, Wang J, Zhang J, et al. PKM2 promotes glucose metabolism and cell growth in gliomas through a mechanism involving a let-7a/c-Myc/hnRNPA1 feedback loop. Oncotarget. 2015;6:13006–18.
28. Gu Z, Xia J, Xu H, Frech I, Tricot G, Zhan F. NEK2 promotes aerobic glycolysis in multiple myeloma through regulating splicing of pyruvate kinase. J Hematol Oncol. 2017;10:17.
29. David CJ, Chen M, Assanah M, Canoll P, Manley JL. HnRNP proteins controlled by c-Myc deregulate pyruvate kinase mRNA splicing in cancer. Nature. 2010;463:364–8.
30. Ning X, Qi H, Li R, Li Y, Jin Y, McNutt MA, et al. Discovery of novel naphthoquinone derivatives as inhibitors of the tumor cell specific M2 isoform of pyruvate kinase. Eur J Med Chem. 2017;138:343–52.
31. Mohagheghi F, Prudencio M, Stuani C, Cook C, Jansen-West K, Dickson DW, et al. TDP-43 functions within a network of hnRNP proteins to inhibit the production of a truncated human SORT1 receptor. Hum Mol Genet. 2016;25:534–45.
32. Roda D, Castillo J, Telechea-Fernandez M, Gil A, Lopez-Rodas G, Franco L. et al. EGF-induced acetylation of heterogeneous nuclear ribonucleoproteins is dependent on KRAS mutational status in colorectal cancer cells. PLoS ONE 2015;10:e0130543
33. Xuan Y, Wang J, Ban L, Lu JJ, Yi C, Li Z, et al. hnRNPA2/B1 activates cyclooxygenase-2 and promotes tumor growth in human lung cancers. Mol Oncol. 2016;10:610–24.
34. Pina JM, Reynaga JM, Truong AAM, Keppetipola NM. Post-translational modifications in polypyrimidine tract binding proteins PTBP1 and PTBP2. Biochemistry. 2018;57:3873–82.
35. Pun KK, Young RT, Wang C, Tam CF, Ho PW. The use of glucagon challenge tests in the diagnostic evaluation of hypoglycemia due to hepatoma and insulinoma. J Clin Endocrinol Metab. 1988;67:546–50.
36. Li H, Xu M, Lee J, He C, Xie Z. Leucine supplementation increases SIRT1 expression and prevents mitochondrial dysfunction and metabolic disorders in high-fat diet-induced obese mice. Am J Physiol Endocrinol Metab. 2012;303:E1234–44.
37. Li L, Yoshitomi H, Wei Y, Qin L, Zhou J, Xu T. et al. Tang-Nai-Kang alleviates pre-diabetes and metabolic disorders and induces a gene expression switch toward fatty acid oxidation in SHR.Cg-Leprcp/NDmcr rats. PLoS ONE 2015;10:e0122024
38. Ampferl R, Rodemann HP, Mayer C, Hofling TTA, Dittmann K. Glucose starvation impairs DNA repair in tumour cells selectively by blocking histone acetylation. Radiother Oncol. 2018;126:465–70.
39. Fang X, Lu G, Ha K, Lin H, Du Y, Zuo Q, et al. Acetylation of TIP60 at K104 is essential for metabolic stress-induced apoptosis in cells of hepatocellular cancer. Exp Cell Res. 2018;362:279–86.
40. Lv L, Li D, Zhao D, Lin R, Chu Y, Zhang H, et al. Acetylation targets the M2 isoform of pyruvate kinase for degradation through chaperone-mediated autophagy and promotes tumor growth. Mol Cell. 2011;42:719–30.
41. Xiong Y, Lei QY, Zhao S, Guan KL. Regulation of glycolysis and gluconeogenesis by acetylation of PKM and PEPCK. Cold Spring Harb Symp Quant Biol. 2011;76:285–9.

42. Chen Y, Huang Q, Liu W, Zhu Q, Cui CP, Xu L, et al. Mutually exclusive acetylation and ubiquitylation of the splicing factor SRSF5 control tumor growth. Nat Commun. 2018;9:2464.
43. Lee JY, Kapur M, Li M, Choi MC, Choi S, Kim HJ, et al. MFN1 deacetylation activates adaptive mitochondrial fusion and protects metabolically challenged mitochondria. J Cell Sci. 2014;127:4954–63.
44. Kashima T, Rao N, David CJ, Manley JL. hnRNP A1 functions with specificity in repression of SMN2 exon 7 splicing. Hum Mol Genet. 2007;16:3149–59.